Environmental Science & Technology

Article

Cite This: Environ. Sci. Technol. 2019, 53, 1509−1517

pubs.acs.org/est

Durable Superhydrophobic/Superoleophilic Graphene-Based Foam for High-Efficiency Oil Spill Cleanups and Recovery

Cheng Chen,[†,‡] Xiaoying Zhu,[†,‡] and Baoliang Chen*[,†,‡]

[†]Department of Environmental Science, Zhejiang University, Hangzhou, Zhejiang 310058, China

[‡]Zhejiang Provincial Key Laboratory of Organic Pollution Process and Control, Hangzhou 310058, China

Supporting Information

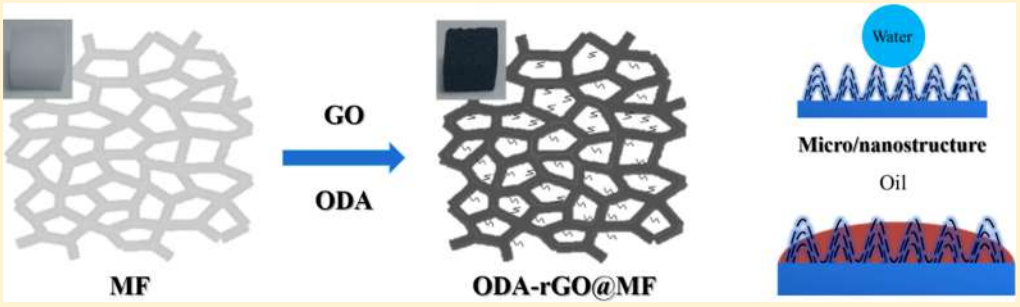

ABSTRACT: One of the most pervasive environmental issues is the frequent oil spills that happen during oil production and transportation processes. This global challenge calls for emerging materials that can effectively separate oil pollutants from water. Here, a facile and feasible method to fabricate a high-performance oil absorbent (ODA-rGO@MF) through the coating of octadecylamine-grafted reduced graphene oxide (ODA-rGO) on the skeleton of commercial melamine foam (MF) is reported. The resultant foam not only possesses the hierarchical pore structure, superior compressibility, and mechanical stability of the original foam but also exhibits high water repellency, superhydrophobicity, and durability under harsh conditions, such as in strongly acidic (alkaline) and salty solutions. The superhydrophobicity of ODA-rGO@MF was created by employing the microarchitecture of MF, forming the rough rGO nanoscale wrinkles on the foam skeletons and further reducing the surface energy by octadecylamine (ODA). These fascinating characteristics make the functionalized foam an excellent oil absorbent with a high absorption capacity (44−111 times its own weight) and extraordinary recyclability. More importantly, the inexpensive materials and low-cost fabrication technique make it possible for large-scale production. Thus, the as-prepared foam has the potential to be used as a promising absorbent for oil-spill cleanups.

1. INTRODUCTION

The exploitation of oil resources has brought great economic benefits to humans. However, frequent oil spills have happened during oil production and transportation processes, usually causing severe damage to the marine ecosystem.[1−3] Such oil pollution has become one of the most urgent global environmental problems. Therefore, the development of methods for the cleanup of various oil pollutants from water is attracting global attention.

A number of conventional methods have been developed for oil spill remediation including solidifiers,[4] in situ burning,[5] chemical dispersants,[6] skimming,[7] and bioremediation.[8] However, these techniques are somewhat time-consuming, high cost, and environmentally unfriendly. Compared with these methods and technologies, using sorbents seems to be a more attractive method for the removal and collection of spilled oils from water due to their low cost and easy accessibility. Oil absorbents, including zeolites,[9] activated carbon,[10] organoclays,[11] exfoliated graphite,[12] wool fibers,[13] kapok fiber,[14] and rice straw,[15] have been widely used in practical applications for the cleanup of oil spills. However, these oil absorbents still suffer from the limits of low water repellency and poor buoyancy, resulting in poor oil/water selectivity (with some pore volume occupied by water) and inconvenient recycling.[16] Therefore, oil absorbents with properties such as high oil absorption capacity, high selectivity, low density, and excellent recyclability are urgently needed.

In recent years, researchers have endeavored to obtain both superhydrophobic and superoleophilic three-dimensional (3D) porous materials owing to their outstanding oil absorption performance and water repelling ability.[17] Generally, such superhydrophobic materials can be prepared by combining micro/nanostructures with low-surface-energy materials.[18] The methods to fabricate superhydrophobic 3D porous materials can be primarily classified into two categories. The first method is constructed through a bottom-up assembly process, e.g., ultralight carbon nanofiber aerogels,[19] carbon nanotube

Received: August 19, 2018
Revised: December 18, 2018
Accepted: January 5, 2019
Published: January 6, 2019

DOI: 10.1021/acs.est.8b04642
Environ. Sci. Technol. 2019, 53, 1509−1517

aerogels,[20] graphene aerogels,[21] graphene-carbon nanotube aerogels,[22] and boron nitride aerogels.[23] The micrometer-scale rough structure of these aerogels has greatly amplified the hydrophobicity of the building blocks (such as carbon nanofibers, graphene, carbon nanotubes, boron nitride, and so on) to superhydrophobicity.[17] Because of the low density, large surface area, and high porosity of these aerogels, they exhibit superior efficiency and recyclability in the cleanup of oil pollutants.[16,24,25] However, there are some drawbacks to which attention should be paid, including the poor mechanical strength, high cost, and complex preparation processes, which restrict their large-scale application.

Compared with the difficulty existing in assembling those nanomaterials into large 3D macrostructures, another method focused on the modification on 3D substrates is considered to be a versatile and cost-efficient approach for the fabrication of oil sorbents.[26] Commercial 3D porous materials with existing microlevel structures, such as PU sponge and melamine sponge, have always been considered as ideal substrates for the fabrication of oil sorbents due to their low density, porous structure, and good elasticity.[27,28] Until the present, a number of materials, including fluorinated compounds,[29] fatty acids,[30] polydimethylsiloxane (PDMS),[31] carbon nanotubes (CNTs),[32] and reduced graphene oxide (rGO),[33,34] have been used to change the wettability of commercial sponges from superhydrophilic to superhydrophobic by increasing the surface roughness and reducing the surface energy. However, the majority of preparation processes for fabricating superhydrophobic surfaces have limitations for large-scale fabrication due to the complicated processes and involved environmentally harmful materials[30,35,36] (e.g., long-chain polyfluorinated compounds), which can lead to bioaccumulation and toxicity.[37] In addition, most of the superhydrophobic/superoleophilic surfaces may lose their superhydrophobic performance when contacted with strong corrosive liquids or salty solutions due to the change in chemical composition or surface structure, thus, limiting their practical application in oil/harsh water conditions.[26] Although several studies concerning anticorrosion hydrophobic coatings for sorbent materials have been reported,[38,39] it is still necessary to develop materials with durable superhydrophobicity through a facile and scalable way for oil-spill cleanups in corrosive solution environments.

Herein, we report a superhydrophobic graphene-based foam via coating octadecylamine-grafted reduced graphene oxide (ODA-rGO) on the skeletons of the commercial melamine foam. The wettability of commercial melamine foam was dramatically changed from superhydrophilic to superhydrophobic, which could be attributed to the micro- and nanostructures created by the stacking of rGO and the low surface energy introduced by the grafted octadecylamine (ODA). The obtained ODA-rGO-wrapped melamine foam (ODA-rGO@MF) exhibited outstanding chemical stability in harsh environments including strongly acidic (or alkaline) and concentrated salty conditions. The superhydrophobic foam can be used to selectively absorb various oils and liquid organic solvents from water with sorption capacities of 44−111 times its own weight. Furthermore, this material can be reused by a simple squeezing process with good recyclability. We believe that this novel oil sorbent has great potential for practical application in oil spill remediation.

2. MATERIALS AND METHODS

2.1. Materials. Graphene oxide (GO) was synthesized from natural graphite flakes (325 mesh, 99.8%, Alfa Aesar) using a modified Hummers' method.[40,41] The detailed process is presented in the Supporting Information. Commercial melamine foams were purchased from Shanghai Foam Materials, Co. Octadecylamine, oils, and organic solvents (chloroform, DMSO, styrene, olive oil, DMF, *o*-xylene, cyclohexane, THF, diesel, toluene, *n*-hexane, and ligarine) were obtained from Aladdin.

2.2. Preparation of the ODA-rGO@MF. The MF was cut into blocks ($1 \times 1 \times 1$ cm^3) and cleaned successively with alcohol and deionized water by sonicating for 3 h. After drying in an oven at 60 °C, the MF blocks were put into a GO suspension (3 mg/mL) and squeezed/released in the GO suspension for 5 min to ensure that MF was absolutely wetted by the GO suspension. The MF foam filled with the GO suspension was taken out and dried at 60 °C for 24 h in an oven to obtain the GO-wrapped MF (GO@MF). The GO@MF was put into an ODA/alcohol solution (4 mg/mL) and slowly squeezed/released 3 times. The GO@MF filled with the ODA/alcohol solution was removed and reacted at 180 °C for 12 h. The obtained foam was washed with alcohol to remove the residual ODA. After drying at 60 °C for 6 h, the final ODA-rGO@MF was obtained. The rGO-wrapped melamine foam (rGO@MF) was prepared by the same process but without the addition of ODA. The whole process is illustrated in Figure 1.

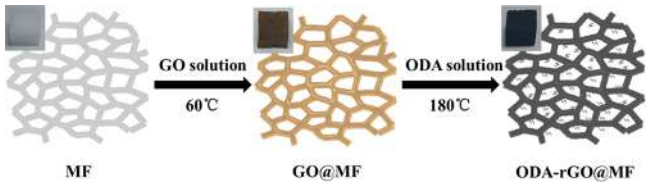

Figure 1. Illustration of the synthetic process of ODA-rGO@MF.

2.3. Oil Sorption of ODA-rGO@MF. The absorption capacity (Q) of ODA-rGO@MF was measured by an oil sorption experiment. Ten kinds of oils and organic solvents were selected including chloroform, DMSO, styrene, olive oil, DMF, *o*-xylene, cyclohexane, THF, diesel, toluene, *n*-hexane, and ligarine. The ODA-rGO@MF was first weighed and then immersed into the oil or organic solvent for 3 min, afterward, the sponge was picked out, drained for 30 s to remove the excess oil, and quickly weighed to avoid evaporation of the oil or organic solvent. The absorption capacity (Q) was calculated with the following equation:

$$Q = (M - M_0)/M_0 \quad (1)$$

where M_0 and M are the masses of ODA-rGO@MF before and after absorption, respectively.

2.4. Recyclability of ODA-rGO@MF. The recyclability of ODA-rGO@MF was evaluated by repeated absorbing-squeezing processes. The absorbing-squeezing process was performed by immersing the ODA-rGO@MF into oil for 3 min and then manually squeezing the sponge to extract the absorbed oil. The absorption capacity of ODA-rGO@MF was measured for each cycle.

2.5. Characterization. The density of the foams (ρ_F) was calculated using the following equation:

DOI: 10.1021/acs.est.8b04642
Environ. Sci. Technol. 2019, 53, 1509−1517

$$\rho_F = \frac{M}{V} \quad (2)$$

where M and V are the weight and volume of the foams, respectively. The porosity of the foams (Φ) was calculated using the formula:

$$\Phi = \left(1 - \rho_F \times \left(\frac{X_M}{\rho_M} + \frac{X_{rGO}}{\rho_{rGO}} + \frac{X_{ODA}}{\rho_{ODA}}\right)\right) \times 100\% \quad (3)$$

where ρ_F, ρ_M, ρ_{rGO}, and ρ_{ODA} are the densities of the foam, melamine, rGO, and ODA, respectively. The X_M, X_{rGO}, and X_{ODA} are the weight percentages of the melamine, rGO, and ODA. The surface morphologies of ODA-rGO@MF and MF were characterized by scanning electron microscopy (SEM, S-4800/SU8010). Before observation, the samples were affixed to a sample stage by conductive tape and coated with gold for 40 s. Atomic force microscopy (AFM) of ODA-rGO was performed in peak force tapping mode on a Bruker Icon. X-ray photoelectron spectroscopy (XPS) was performed on a VG Escalab Mark II with a resolution of less than 0.2 eV. The C ls peak spectra were analyzed using XPS Peak 4.1 software. Fourier transform infrared (FTIR) spectra were recorded in the 4000−400 cm^{-1} region by averaging 64 scans, at 1 min intervals to minimize the effects of dynamic scanning, at a resolution of 4 cm^{-1} using a Bruker Vector 22FTIR spectrometer. Raman experiments were performed on a LabRAM HR UV spectrometer (Horiba Jobin Yvon) with excitation by the 514.5 nm line from an Ar^+ laser and a resolution of 1.0 cm^{-1}. Water contact angle (WCA) measurements were performed on an OSA Optical Surface Analyzer-OSA200-B. All contact angle values were determined by the TrueDrop method in the software. Five different locations of the surface were examined to obtain the average value.

3. RESULTS AND DISCUSSION

3.1. Structural Characteristics of ODA-rGO@MF. The morphologies of pure MF and ODA-rGO@MF were observed by SEM. As shown in Figure 2a, the pure MF showed an interconnected porous structure with pore diameters ranging from tens to hundreds of micrometers, which is important for the internal transmission and circulation of matter. The smooth skeleton of pure MF can be observed in Figure 2b. After coating with ODA-rGO (Figure 2c), the porous structure was well maintained, indicating that the existing microlevel porous structures of MF were fully inherited by ODA-rGO@MF with no apparent damage occurring during the coating process. The morphologies inside and outside the foam are nearly the same with most of the ODA-rGO sheets wrapped around the skeletons of the foam (Figure S1). Meanwhile, the packing and stacking of the irregular ODA-rGO on the skeletons of MF can be observed in Figure 2d and Figure S2. The surface roughness of the foam skeleton was notably increased, and several micro/nanoscale protrusions and wrinkles on the skeletons were present. Thus, the as-expected multiscale rough structure was successfully formed, which is of great importance for altering the wettability of the MF to be superhydrophobic.

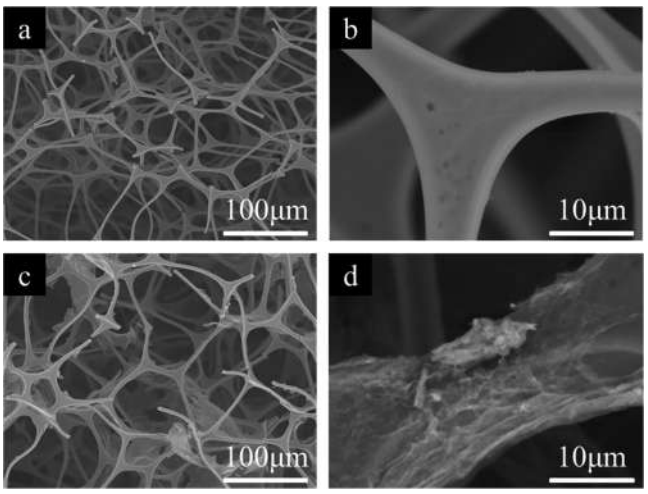

Figure 2. External SEM images of pure MF (a and b) and ODA-rGO@MF (c and d).

The successful coating of ODA-rGO on the skeletons of MF was further confirmed through XPS for the analysis of the surface chemical composition. As shown in Figure 3a, the three characteristic peaks at 284.6, 400.6, and 531.6 eV were attributed to the C 1s, N 1s, and O 1s of MF.[42] Compared with the spectrum for MF, the intensity of C 1s in ODA-rGO@MF was clearly increased, but the N 1s peak and O 1s peak were relatively decreased. This phenomenon indicates that ODA-rGO was successfully coated on the surface of the MF skeletons. The C 1s peak of MF and ODA-rGO@MF was deconvoluted into four peaks at binding energies of 284.6 eV (C═C), 286.1 eV (C−O), 287.6 eV (C−N), and 288.9 eV (C═O) (Figure 3b and c).[43,44] The relative content of each form of C species is listed in Table S1, which was calculated from the XPS-peak-differentiation-imitating analysis. The highest content of C−N presented in MF can be explained by the triazine ring in the skeleton. After coating ODA-rGO on the surface of the skeleton, the C−N from the triazine ring was sheltered by the ODA-rGO, which consists of graphitic carbon in rGO and alkyl carbon in ODA. Thus, the relative content of C−C significantly increased, but the relative content of C−N decreased.

The FTIR spectra of GO, ODA-rGO, MF, and ODA-rGO@MF are shown in Figure 3d. The strong peaks at 1693, 1609, 1402, 1203, and 1039 cm^{-1} in the GO spectrum were associated with O−H, C═O, C−O−C (epoxy), and C−O (alkoxy) bonds, which is consistent with several previous works.[45,46] In the ODA-rGO spectrum, the intensities of the oxygen functional groups (including O−H, C═O, and C−O (alkoxy)) clearly decreased, indicating the reduction of GO to rGO with most of the oxygen functional groups removed. The newly formed peaks at 2918, 2846, and 1459 cm^{-1} were attributed to the C−H stretching and deformation, resulting from the introduction of the long hydrocarbon chain from ODA.[47] The broad peak at 1191 cm^{-1} was explained by the nucleophilic ring-opening reaction between the C−O−C (epoxy) in GO and $-NH_2$ in ODA. The C−O (epoxy and alcohol) and C−N peaks were overlapped in the same region of wavenumbers.[48] Thus, the broad peak at 1191 cm^{-1} was formed for ODA-rGO.

For the pure MF, the prominent peaks at 810, 1545, 1693, and 3400 cm^{-1} were assigned to triazine ring bending, C═N stretching, C═O stretching, and the stretching vibration of N−H or O−H, respectively.[49] The peaks centered at 1316 and 1452 cm^{-1} were indicative of C−H bending.[50] Moreover, two small peaks at 2846 and 2918 cm^{-1} were attributed to C−H stretching.[47] After coating with ODA-rGO, the peaks of C−H

DOI: 10.1021/acs.est.8b04642
Environ. Sci. Technol. 2019, 53, 1509−1517

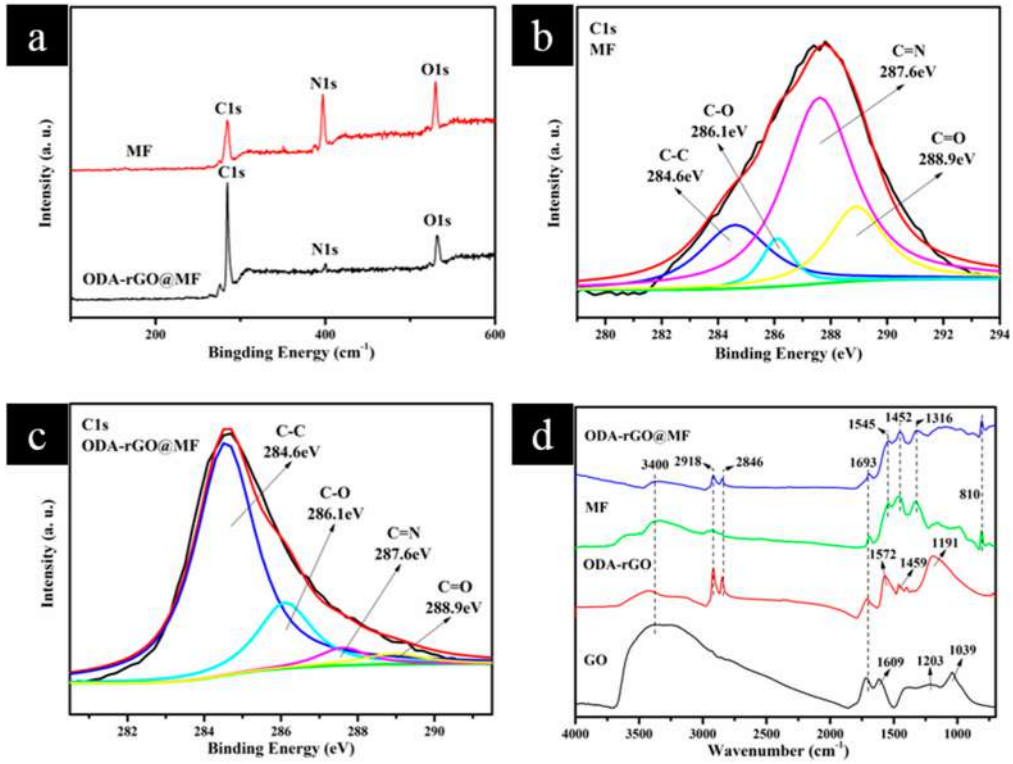

Figure 3. (a) XPS survey profiles of MF and ODA-rGO@MF. Deconvolution of the XPS C 1s for (b) MF and (c) ODA-rGO@MF. (d) FTIR spectra of GO, ODA-rGO, MF, and ODA-rGO@MF.

bending and stretching strengthened significantly in intensity, whereas the peaks of triazine ring bending, C═N stretching, and C═O stretching weakened for ODA-rGO@MF, which indicated that the skeleton of MF was coated by ODA-rGO.

All these results indicated that the surface morphology and surface chemical composition of the skeleton in MF were completely changed during the preparation process. In the beginning, the skeleton was covered by GO nanosheets due to their 2D flexible lamellar structure. After heating at 180 °C and reacting with ODA, the micro/nanostructured skeleton was formed as a result of the stacking and wrinkling of the irregular rGO nanosheets. Meanwhile, ODA was introduced on the surface of rGO, which was used here to further reduce the surface energy. After grafting, octadecyl groups are exposed rather than the residual hydrophilic oxygen-containing functional groups on rGO sheets. Therefore, the ODA-rGO was considered to have a relatively low surface energy. Thus, the as-expected foam was successfully prepared with a micro/nanostructure and reduced surface energy, which were necessary for achieving superhydrophobicity.[51]

3.2. Wettability of the ODA-rGO@MF. The wettability of the ODA-rGO@MF and rGO@MF was characterized by water contact angle measurements. As shown in Figure 4a, the water contact angle of the rGO@MF was always lower than 150°. After the introduction of ODA, the water contact angle of the ODA-rGO@MF increased, confirming that ODA can strengthen the hydrophobicity of rGO. The value reached a maximum of 153.5° when the concentration of GO increased to 3 mg/mL, indicating the superhydrophobic characteristics of the functionalized foam. The slight decrease in the water contact angle from 3 mg/mL to 5 mg/mL can be attributed to the smooth external surface formed by the stacking of excess rGO, as shown in Figure S3. The relationship between the concentration of ODA and the water contact angle of the ODA-rGO@MF is shown in Figure 4b. The value of the water contact angle notably increased as a function of the concentration of ODA from 0.5 mg/mL to 4 mg/mL and remained nearly unchanged from 4 mg/mL to 6 mg/mL due to the limited number of reaction sites on GO. Thus, 3 mg/mL of the GO suspension and 4 mg/mL of the ODA/alcohol solution were selected as the optimal concentrations to prepare the ODA-rGO@MF.

The water repellency of the ODA-rGO@MF can be observed in Figure 4c. In a water bath, the hydrophilic pure MF sank to the bottom, while the superhydrophobic ODA-rGO@MF floated. When immersing the ODA-rGO@MF in water by external force, a mirror-like interface formed between the surface of the sponge and the surrounding water due to the entrapped air residing in the rough surface of the ODA-rGO@MF. This phenomenon can be referred to as a so-called nonwetting Cassie−Baxter surface.[52] Figure 4d, e, and f shows that both water droplets and oil droplets were completely absorbed by the pure MF due to its superhydrophilicity. In contrast, the water droplet remained on the surface of the ODA-rGO@MF and was nearly perfectly spherical (Figure 4g and h), while the oil droplet spread-out completely and penetrated into the pores of the material within one second (Figure 4i). These results indicated the successful surface modification of MF from superhydrophilic to superhydrophobic. The superhydrophobicity and superoleophilicity of the ODA-rGO@MF are illustrated in Figure 4j and k. Due to the as-formed micro/nanostructures, air was trapped among these hierarchical rough structures, which could not be wetted by the water. Thus, the ODA-rGO@MF showed a relatively high

DOI: 10.1021/acs.est.8b04642
Environ. Sci. Technol. 2019, 53, 1509−1517

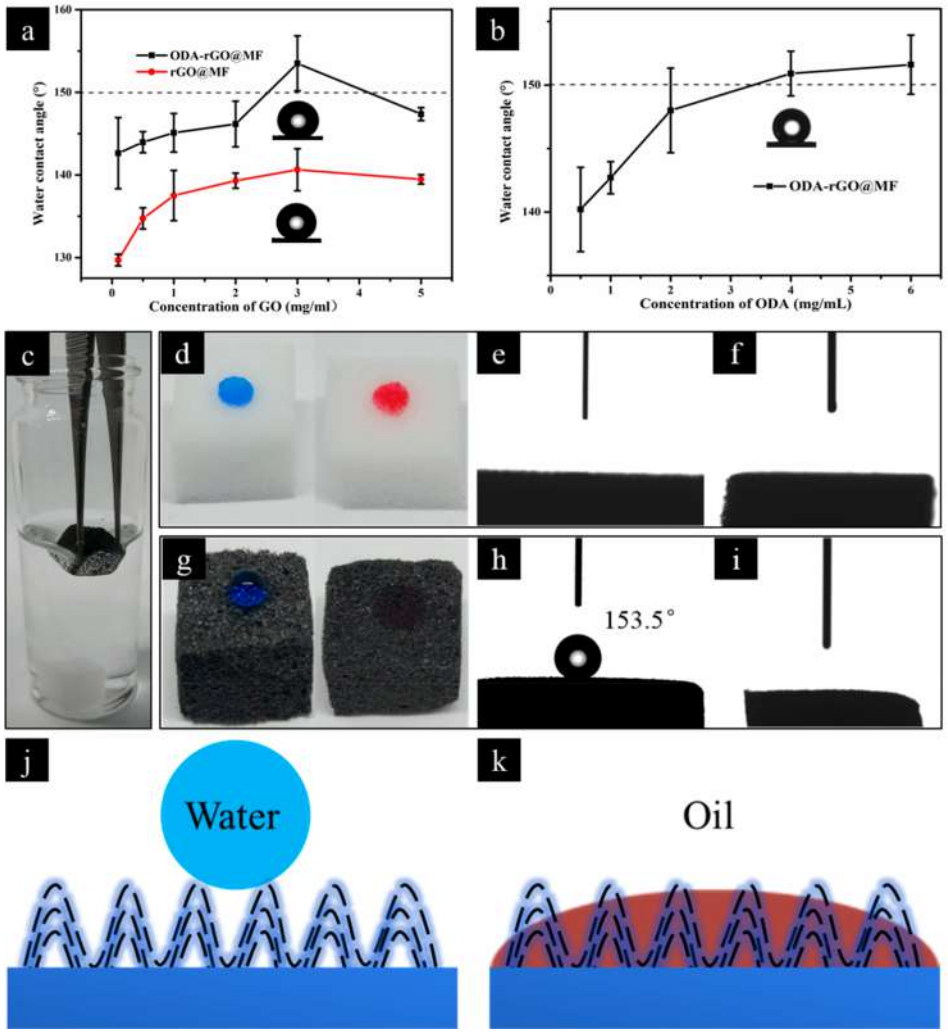

Figure 4. (a) Relationship between the concentration of GO (0.1−5 mg/mL) and the water contact angle of ODA-rGO@MF and rGO@MF with the concentration of ODA fixed at 4 mg/mL. (b) The relationship between the concentration of ODA (0.5−6 mg/mL) and the water contact angle of ODA-rGO@MF with the concentration of GO fixed at 3 mg/mL. (c) A picture of the white MF at the bottom of a bottle and black ODA-rGO@MF immersed into water by an external force. A picture of water droplets (on the left, dyed with methylene blue) and oil droplets (on the right, dyed with Sudan III) on the surfaces of the MF (d) and ODA-rGO@MF (g). The water and oil contact angles of the MF (e and f) and ODA-rGO@MF (h and i). Schematic illustration of the superhydrophobicity (j) and superoleophilicity (k) of the ODA-rGO@MF.

static water contact angle. Different from the water droplet, the oil droplet can easily wet the hierarchical rough structures because of the capillary effect. Therefore, the ODA-rGO@MF showed superoleophilicity with a low oil contact angle.

Based on the above results, the surface of ODA-rGO@MF can be considered to be composed of ODA-rGO and air. Therefore, the Cassie equation,[53] $\cos\theta^* = f\cos\theta + f - 1$, was applied to calculate the ratio of the combined water−solid and air−solid interface areas to the apparent surface area. Herein, θ^* is the apparent contact angle of the ODA-rGO@MF, θ is the intrinsic water contact angle of the ODA-rGO, f represents the area fraction of the superhydrophobic surface that is in contact with water, and $1 - f$ represents the area fraction of the trapped air on the superhydrophobic surface. The intrinsic water contact angle value of the ODA-rGO was 101.4°, which is shown in Figure S4 d. Only 9.9% of the superhydrophobic surface was wetted by water, which means that 90.1% of the area was occupied by trapped air among these hierarchical structures. Therefore, most of the water contacted air rather than the surface of the ODA-rGO@MF, resulting from the large amount of air that was trapped in the "pockets" between the liquid and the solid substrate.[54] This result was quite consistent with the dynamic wetting behavior of the ODA-rGO@MF, which was investigated through the measuring of the advancing/receding contact angle and tilt angle. The advancing/receding contact angle of the ODA-rGO@MF was measured by increasing the water droplet volume at a rate of 0.1 μL/s. As shown in Figure S5a and b, the ODA-rGO@MF gave advancing and receding water contact angles of 156.7° and 147.2°, respectively. This was in agreement with the static water contact angle (153.5°, shown in Figure 4h), which should lie between the advancing and receding angle values.[55] The water contact angle hysteresis (which is the difference between the advancing and receding values) for the ODA-rGO@MF was 9.5°, suggesting the lower adhesion of water on the surface of the ODA-rGO@MF.[56] To investigate the mobility of the water droplet on the surface of the ODA-rGO@MF, we performed a water droplet rolling experiment by tilting the sample substrate (Figure S5c and d). The tilt angle of the water droplet on the ODA-rGO@MF was 23.5°, at

DOI: 10.1021/acs.est.8b04642
Environ. Sci. Technol. 2019, 53, 1509−1517

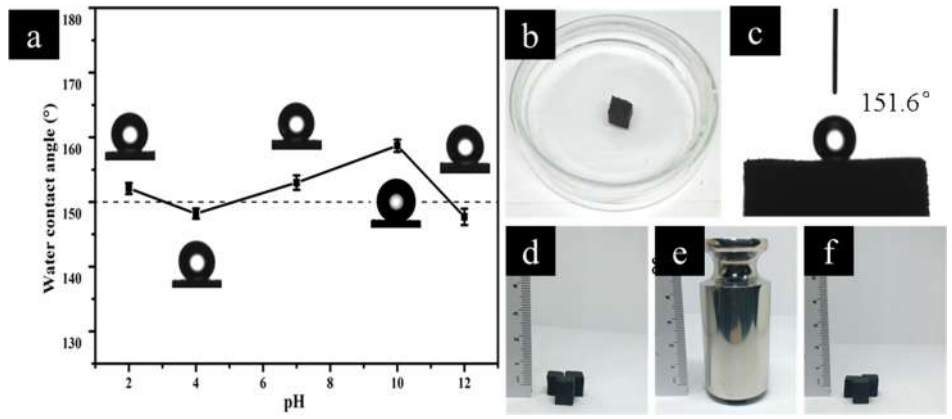

Figure 5. (a) The water contact angle (CA) of the ODA-rGO@MF after immersing in solutions with different pH. (b) Pictures of the ODA-rGO@MF immersed in 0.6 mol/L NaCl. (c) The water contact angle (CA) of the ODA-rGO@MF after immersing in 0.6 mol/L NaCl for 12 h. (d) Optical images showing three ODA-rGO@MF samples ($1 \times 1 \times 1$ cm^3), (e) which support >12,000 times its own weight with approximately 80% strain. (f) The full recovery with no evident permanent deformation when unloading.

which the water droplet spontaneously rolled off the surface. All these results indicated the superhydrophobicity and low adhesion of water to the ODA-rGO@MF.

3.3. Stability of the ODA-rGO@MF. Despite a multitude of superhydrophobic materials that have been prepared, the stability of these materials has often been overlooked. Herein, the stability of the ODA-rGO@MF was investigated by immersing a sample into an aqueous solution with pH in the range from 2 to 12 for 12 h (Figure 5a). In strong acidic solution, the slight decrease may be due to the tiny H^+ absorbed on the surface of ODA-rGO@MF by electrostatic interaction, while, in strong alkaline solution, the ionization of residual carboxyl groups and phenolic hydroxyl groups in ODA-rGO increased the hydrophilicity of ODA-rGO@MF. Therefore, the slight decrease of water contact angle value at pH 12 can also be observed. Even so, all of the water contact angle values remained approximately 150°, indicating the high stability under corrosive solution conditions. The excellent chemical stability of the ODA-rGO@MF can be attributed to the chemical inertness of rGO and the strong covalent bonding between ODA and rGO. Thus, the chemical composition of the ODA-rGO@MF could not be damaged, even under strong acidic and alkaline solution conditions.

Additionally, we tested the stability of the ODA-rGO@MF in a 0.6 mol/L NaCl solution with high ionic strength (Figure 5b). After 12 h, the retained superhydrophobicity was observed (Figure 5c), suggesting that the ODA-rGO@MF has the potential to be used under ocean conditions. The mechanical strength of the ODA-rGO@MF was tested by loading a 500 g weight on three ODA-rGO@MF samples ($1 \times 1 \times 1$ cm^3), as shown in Figure 5d, e, and f. They could support more than 12,000 times their own weight with approximately 80% strain, indicating the high specific strength. When unloading, the foam fully recovered with no apparent permanent deformation. Besides, the porous structure of ODA-rGO@MF was well maintained, and the rGO sheets never came off from the skeletons after 100 absorbing-squeezing processes (Figure S6), indicating the good stability of the coating.

3.4. Oil Absorption Capacity. The above results show that the ODA-rGO@MF is superhydrophobic and highly stable in many harsh situations. Thus, it has great potential to be used as an excellent sorbent for the selective absorption of oil pollutants from water. When the ODA-rGO@MF was placed on a cyclohexane oil−water mixture (Figure 6a), the 500 μL of cyclohexane oil was selectively absorbed in ~5 s

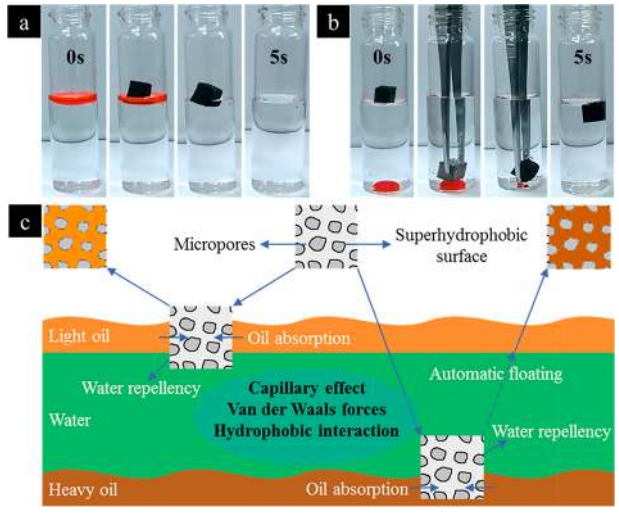

Figure 6. (a) Pictures showing the absorption process of 500 μL of cyclohexane (dyed with Sudan IV) on water by the ODA-rGO@MF. (b) Pictures showing the absorption process of 500 μL of dichloromethane (dyed with Sudan IV) on water by the ODA-rGO@MF. (c) A schematic procedure of the selective oil absorption from water.

with an ultrafast absorption rate of ~100 μL/s, indicating the fascinating efficiency in oil absorption of the material. Once removed, the oil existing in the ODA-rGO@MF could be easily recovered by simple squeezing, resulting in clean water that was the same as the uncontaminated water. As shown in Figure 6b, the ODA-rGO@MF could also effectively absorb a high-density oil pollutant (dichloromethane) from the water. When the ODA-rGO@MF was forced into water and contacted the dichloromethane, the dichloromethane was quickly absorbed by the ODA-rGO@MF within ~5 s. Interestingly, after the absorption, the ODA-rGO@MF could automatically float to the surface due to its water repellency and low density (Table S2), which facilitated its facile collection. This phenomenon suggests that the ODA-rGO@MF should be a promising candidate for the removal of high-density oil pollutants from oil-spilled water.

DOI: 10.1021/acs.est.8b04642
Environ. Sci. Technol. 2019, 53, 1509−1517

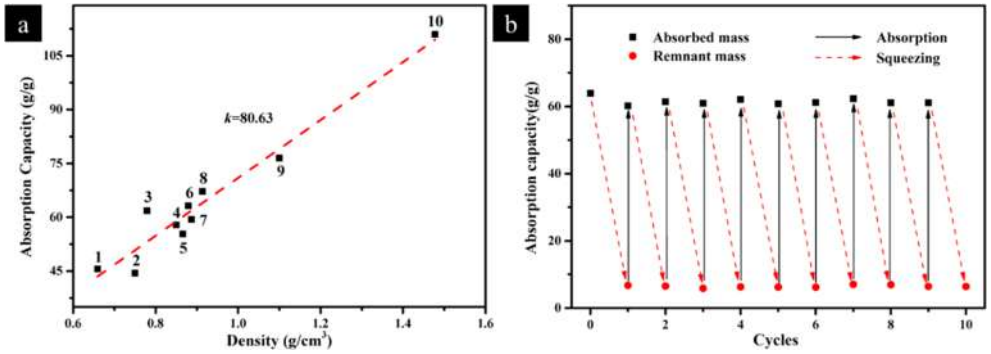

Figure 7. (a) The relationship between absorption capacity (Q) to the densities (ρ) of the oils and organic solvents absorbed by the ODA-rGO@MF (ρ_F = 0.0123 g/cm^3). The numbers (1−10) represent ligarine, *n*-hexane, toluene, diesel, THF, cyclohexane, *o*-xylene, DMF, olive oil, styrene, DMSO, and chloroform, respectively. (b) The absorption recyclability of the ODA-rGO@MF for cyclohexane by manual squeezing.

Based on the above results, the whole absorption process is schematically demonstrated in Figure 6c. The superhydrophobicity of the ODA-rGO@MF can be attributed to the rough micro/nanostructured skeleton and low surface energy formed by the coated rGO and subsequently grafted ODA. Thus, the material shows a high water repellency and oleophilicity, which are of great importance for selective oil absorption from oil-spilled water. When the superhydrophobic ODA-rGO@MF, with a large number of micropores, was placed into the oil-polluted water, the oil occupied the pore space by expelling the air captured in the foam due to the capillary effect, van der Waals forces, and hydrophobic interaction.[16] Different from the ultrafast oil absorption, water was repelled from the pores due to the superhydrophobicity of the ODA-rGO@MF. Thus, during the whole process, the air-filled foam was transformed into oil-filled foam with a negligible amount of water adhering to its surface.

The absorption capacity of MF, rGO@MF, and ODA-rGO@MF for the water and *n*-hexane was shown in Figure S7. The better selectivity of ODA-rGO@MF compared with MF and rGO@MF made it a better choice for selectively absorbing oil from water. Therefore, we measured the absorption capacity (Q) of the ODA-rGO@MF for various oils and organic solvents. As shown in Figure 7a, the ODA-rGO@MF could absorb various oils and organic solvents at 44−111 times its own weight. The oil absorption capacity was linearly dependent on the density of these oils and organic solvents. Since the pore volume was occupied by expelling the air during the absorption process. This phenomenon can be explained by the following formula:[57]

$$Q = \frac{(M - M_0)}{M_0} = \frac{\rho V \Phi + M_{air}}{\rho_F V} = \frac{\Phi}{\rho_F}\rho + A \quad (4)$$

Therefore, the porosity of the ODA-rGO@MF (Φ) is correlated with the slope of the fitting line (k), which was calculated to be 99.17%. This result was in accordance with the tested porosity (99.18%) shown in Table S2. The Q values of the ODA-rGO@MF tested here were larger than the values of several other previously reported absorbents such as nickel foam (3.5 times),[58] PDMS-graphene foam (2−8 times),[59] PU sponge (15−25 times),[60] and silylated nanofibrillated cellulose sponge (49−102 times).[61] The comparison of various oil absorbents with ODA-rGO@MF was summarized in Table S3 of the Supporting Information, even though the absorption capacity of the ODA-rGO@MF was lower than some other graphene-based absorbents such as graphene/EDA foam (100−250 times),[57] cellulose/graphene aerogel (80−197 times),[62] and CNT/graphene hybrid aerogel (100−322 times).[63] The fabrication process of our graphene-based foam is facile and easy to scale up due to the low-cost fabrication technique and less use of expensive graphene. The recyclability of an oil absorbent also plays an important role in oil cleanup applications. Herein, the absorbed oils were harvested through manual squeezing. Figure 7b shows the recyclable use of the ODA-rGO@MF for the absorption of different kinds of oil. From the second cycle, the saturated absorption capacity remained at ∼95.8% of the absorption capacity in the first cycle. Such a negligible decrease can be attributed to the residual oil inside the sponge, which cannot be removed by manual squeezing. The above results show that the ODA-rGO@MF has not only a high absorption capacity for various oils but also a good recyclability.

In summary, the novel superhydrophobic and superoleophilic ODA-rGO@MF was successfully fabricated through coating rGO on the surface of an MF skeleton to create a micro/nanostructure and through introducing ODA to further reduce the surface energy. The as-prepared ODA-rGO@MF exhibited many outstanding characteristics, including water repellency, superhydrophobicity, stability in corrosive solutions with pH values ranging from 2 to 12 and in salty conditions, excellent elasticity, and a high selective absorption capacity up to 44−111 times its own weight. Furthermore, the ODA-rGO@MF could be recycled by a simple squeezing process and retained its high absorption capacity. Because of the inexpensive materials, scalable fabrication technique, and excellent performance, this superhydrophobic ODA-rGO@MF will be a promising candidate for the selective removal of oil from water.

■ ASSOCIATED CONTENT

Supporting Information

The Supporting Information is available free of charge on the ACS Publications website at DOI: 10.1021/acs.est.8b04642.

Preparation of graphene oxide; Figures S1−S3 and S6, SEM images; Figure S4, AFM 2D image; Figure S5, water contact angles; Figure S7, absorption capacity; Table S1, relative content of each form of C species; Table S2, density and porosity; Table S3, comparison of oil absorbents (PDF)

DOI: 10.1021/acs.est.8b04642
Environ. Sci. Technol. 2019, 53, 1509−1517

AUTHOR INFORMATION

Corresponding Author

*Phone: +86-571-8898-2587. Fax: +86-571-8898-2587. E-mail: blchen@zju.edu.cn.

ORCID

Xiaoying Zhu: 0000-0002-3272-341X

Baoliang Chen: 0000-0001-8196-081X

Notes

The authors declare no competing financial interest.

ACKNOWLEDGMENTS

This project was supported by the National Natural Science Foundation of China (Grants number 21425730, 21537005, and 21621005) and the National Basic Research Program of China (Grant 2014CB441106).

REFERENCES

(1) Schrope, M. Oil cruise finds deep-sea plume. *Nature* **2010**, *465* (7296), 274−275.

(2) Schrope, M. Oil spill: Deep wounds. *Nature* **2011**, *472* (7342), 152−154.

(3) Schrope, M. The lost legacy of the last great oil spill. *Nature* **2010**, *466* (7304), 304−305.

(4) Basak, S.; Nanda, J.; Banerjee, A. A new aromatic amino acid based organogel for oil spill recovery. *J. Mater. Chem.* **2012**, *22* (23), 11658−11664.

(5) Aurell, J.; Gullett, B. K. Aerostat sampling of PCDD/PCDF emissions from the Gulf oil spill in situ burns. *Environ. Sci. Technol.* **2010**, *44* (24), 9431−9437.

(6) Kujawinski, E. B.; Kido Soule, M. C.; Valentine, D. L.; Boysen, A. K.; Longnecker, K.; Redmond, M. C. Fate of dispersants associated with the deepwater horizon oil spill. *Environ. Sci. Technol.* **2011**, *45* (4), 1298−1306.

(7) Broje, V.; Keller, A. A. Improved mechanical oil spill recovery using an optimized geometry for the skimmer surface. *Environ. Sci. Technol.* **2006**, *40* (24), 7914−7918.

(8) Zahed, M. A.; Aziz, H. A.; Isa, M. H.; Mohajeri, L.; Mohajeri, S. Optimal conditions for bioremediation of oily seawater. *Bioresour. Technol.* **2010**, *101* (24), 9455−9460.

(9) Rajaković-Ognjanović, V.; Aleksić, G.; Rajaković, L. Governing factors for motor oil removal from water with different sorption materials. *J. Hazard. Mater.* **2008**, *154* (1), 558−563.

(10) Okiel, K.; El-Sayed, M.; El-Kady, M. Y. Treatment of oil−water emulsions by adsorption onto activated carbon, bentonite and deposited carbon. *Egypt. J. Pet.* **2011**, *20* (2), 9−15.

(11) Carmody, O.; Frost, R.; Xi, Y.; Kokot, S. Adsorption of hydrocarbons on organo-clays—Implications for oil spill remediation. *J. Colloid Interface Sci.* **2007**, *305* (1), 17−24.

(12) Toyoda, M.; Aizawa, J.; Inagaki, M. Sorption and recovery of heavy oil by using exfoliated graphite. *Desalination* **1998**, *115* (2), 199−201.

(13) Radetic, M. M.; Jocic, D. M.; Jovancic, P. M.; Petrovic, Z. L.; Thomas, H. F. Recycled wool-based nonwoven material as an oil sorbent. *Environ. Sci. Technol.* **2003**, *37* (5), 1008−1012.

(14) Wang, J. T.; Zheng, Y.; Wang, A. Q. Effect of kapok fiber treated with various solvents on oil absorbency. *Ind. Crops Prod.* **2012**, *40* (3), 178−184.

(15) Sun, X. F.; Sun, R.; Sun, J. X. Acetylation of rice straw with or without catalysts and its characterization as a natural sorbent in oil spill cleanup. *J. Agric. Food Chem.* **2002**, *50* (22), 6428−6433.

(16) Liu, H. Z.; Geng, B. Y.; Chen, Y. F.; Wang, H. Y. Review on the aerogel-type oil sorbents derived from nanocellulose. *ACS Sustainable Chem. Eng.* **2017**, *5* (1), 49−66.

(17) Zhang, W. F.; Liu, N.; Cao, Y. Z.; Lin, X.; Liu, Y. N.; Feng, L. Superwetting porous materials for wastewater treatment: from immiscible oil/water mixture to emulsion separation. *Adv. Mater. Interfaces* **2017**, *4* (10), 1600029.

(18) Tian, Y.; Su, B.; Jiang, L. Interfacial material system exhibiting superwettability. *Adv. Mater.* **2014**, *26* (40), 6872−6897.

(19) Wu, Z. Y.; Li, C.; Liang, H. W.; Chen, J. F.; Yu, S. H. Ultralight, flexible, and fire-resistant carbon nanofiber aerogels from bacterial cellulose. *Angew. Chem.* **2013**, *125* (10), 2997−3001.

(20) Gui, X.; Wei, J.; Wang, K.; Cao, A.; Zhu, H.; Jia, Y.; Shu, Q.; Wu, D. Carbon nanotube sponges. *Adv. Mater.* **2010**, *22* (5), 617−621.

(21) Sun, H.; Xu, Z.; Gao, C. Multifunctional, ultra-flyweight, synergistically assembled carbon aerogels. *Adv. Mater.* **2013**, *25* (18), 2554−2560.

(22) Chen, L.; Du, R.; Zhang, J.; Yi, T. Density controlled oil uptake and beyond: from carbon nanotubes to graphene nanoribbon aerogels. *J. Mater. Chem. A* **2015**, *3* (41), 20547−20553.

(23) Song, Y.; Li, B.; Yang, S.; Ding, G.; Zhang, C.; Xie, X. Ultralight boron nitride aerogels via template-assisted chemical vapor deposition. *Sci. Rep.* **2015**, *5*, 10337.

(24) Shen, Y.; Fang, Q.; Chen, B. Environmental applications of three-dimensional graphene-based macrostructures: Adsorption, transformation, and detection. *Environ. Sci. Technol.* **2015**, *49* (1), 67−84.

(25) Gupta, S.; Tai, N. H. Carbon materials as oil sorbents: a review on the synthesis and performance. *J. Mater. Chem. A* **2016**, *4* (5), 1550−1565.

(26) Ge, J.; Zhao, H. Y.; Zhu, H. W.; Huang, J.; Shi, L. A.; Yu, S. H. Advanced sorbents for oil-spill cleanup: Recent advances and future perspectives. *Adv. Mater.* **2016**, *28* (47), 10459−10490.

(27) Ge, J.; Ye, Y. D.; Yao, H. B.; Zhu, X.; Wang, X.; Wu, L.; Wang, J. L.; Ding, H.; Yong, N.; He, L. H.; Yu, S. H. Pumping through porous hydrophobic/oleophilic materials: An alternative technology for oil spill remediation. *Angew. Chem., Int. Ed.* **2014**, *53* (14), 3612−3616.

(28) Cheng, M. J.; Ju, G. N.; Jiang, C.; Zhang, Y. J.; Shi, F. Magnetically directed clean-up of underwater oil spills through a functionally integrated device. *J. Mater. Chem. A* **2013**, *1* (43), 13411−13416.

(29) Ogihara, H.; Xie, J.; Saji, T. Controlling surface energy of glass substrates to prepare superhydrophobic and transparent films from silica nanoparticle suspensions. *J. Colloid Interface Sci.* **2015**, *437*, 24−27.

(30) Wang, H. Y.; Wang, E. Q.; Liu, Z. J.; Gao, D.; Yuan, R. X.; Sun, L. Y.; Zhu, Y. J. A novel carbon nanotubes reinforced superhydrophobic and superoleophilic polyurethane sponge for selective oil-water separation through a chemical fabrication. *J. Mater. Chem. A* **2015**, *3* (1), 266−273.

(31) Xi, P. X.; Huang, L.; Xu, Z. H.; Chen, F. J.; An, L.; Wang, B.; Chen, Z. N. Low cost and robust soot dipped polyurethane sponge for highly efficient and recyclable oil and organic solvent cleanup. *RSC Adv.* **2014**, *4* (103), 59481−59485.

(32) Wang, C. F.; Lin, S. J. Robust superhydrophobic/superoleophilic sponge for effective continuous absorption and expulsion of oil pollutants from water. *ACS Appl. Mater. Interfaces* **2013**, *5* (18), 8861−8864.

(33) Liu, Y.; Ma, J.; Wu, T.; Wang, X.; Huang, G.; Liu, Y.; Qiu, H.; Li, Y.; Wang, W.; Gao, J. Cost-effective reduced graphene oxide-coated polyurethane sponge as a highly efficient and reusable oil-absorbent. *ACS Appl. Mater. Interfaces* **2013**, *5* (20), 10018−10026.

(34) Song, S.; Yang, H.; Su, C. P.; Jiang, Z. B.; Lu, Z. Ultrasonic-microwave assisted synthesis of stable reduced graphene oxide modified melamine foam with superhydrophobicity and high oil adsorption capacities. *Chem. Eng. J.* **2016**, *306*, 504−511.

(35) Ruan, C.; Ai, K.; Li, X.; Lu, L. A superhydrophobic sponge with excellent absorbency and flame retardancy. *Angew. Chem., Int. Ed.* **2014**, *53* (22), 5556−5560.

(36) Zhang, X.; Li, Z.; Liu, K.; Jiang, L. Bioinspired multifunctional foam with self-cleaning and oil/water separation. *Adv. Funct. Mater.* **2013**, *23* (22), 2881−2886.

DOI: 10.1021/acs.est.8b04642
Environ. Sci. Technol. 2019, 53, 1509−1517

(37) Darmanin, T.; Guittard, F. Superoleophobic surfaces with short fluorinated chains? *Soft Matter* **2013**, *9* (25), 5982−5990.
(38) Yu, Y.; Chen, H.; Liu, Y.; Craig, V. S. J.; Wang, C.; Li, L. H.; Chen, Y. Superhydrophobic and superoleophilic porous boron nitride nanosheet/polyvinylidene fluoride composite material for oil-polluted water cleanup. *Adv. Mater. Interfaces* **2015**, *2* (1), 1400267.
(39) Wang, J.; Wang, H.; Geng, G. Highly efficient oil-in-water emulsion and oil layer/water mixture separation based on durably superhydrophobic sponge prepared via a facile route. *Mar. Pollut. Bull.* **2018**, *127*, 108−116.
(40) Hummers, W. S.; Offeman, R. E. Preparation of graphitic oxide. *J. Am. Chem. Soc.* **1958**, *80* (6), 1339−1339.
(41) Kovtyukhova, N. I.; Ollivier, P. J.; Martin, B. R.; Mallouk, T. E.; Chizhik, S. A.; Buzaneva, E. V.; Gorchinskiy, A. D. Layer-by-layer assembly of ultrathin composite films from micron-sized graphite oxide sheets and polycations. *Chem. Mater.* **1999**, *11* (3), 771−778.
(42) Song, B.; Zhao, J. X.; Wang, M. J.; Mullavey, J.; Zhu, Y. T.; Geng, Z. S.; Chen, D. C.; Ding, Y.; Moon, K. S.; Liu, M. L.; Wong, C. P. Systematic study on structural and electronic properties of diamine/triamine functionalized graphene networks for supercapacitor application. *Nano Energy* **2017**, *31*, 183−193.
(43) Feng, D. M.; Zhou, Z. M.; Bo, M. P. An investigation of the thermal-degradation of melamine phosphonite by XPS and thermal-analysis techniques. *Polym. Degrad. Stab.* **1995**, *50* (1), 65−70.
(44) Shen, Y.; Zhu, X.; Chen, B. Size effects of graphene oxide nanosheets on the construction of three-dimensional graphene-based macrostructures as adsorbents. *J. Mater. Chem. A* **2016**, *4* (31), 12106−12118.
(45) Wang, J.; Chen, B.; Xing, B. Wrinkles and folds of activated graphene nanosheets as fast and efficient adsorptive sites for hydrophobic organic contaminants. *Environ. Sci. Technol.* **2016**, *50* (7), 3798−3808.
(46) Shen, Y.; Chen, B. Sulfonated graphene nanosheets as a superb adsorbent for various environmental pollutants in water. *Environ. Sci. Technol.* **2015**, *49* (12), 7364−7372.
(47) Basiuk, E. V.; Ochoa-Olmos, O.; Contreras-Torres, F. F.; Meza-Laguna, V.; Alvarez-Zauco, E.; Puente-Lee, I.; Basiuk, V. A. "Green" functionalization of pristine multi-walled carbon nanotubes with long-chain aliphatic amines. *J. Nanosci. Nanotechnol.* **2011**, *11* (6), 5546−5554.
(48) Lin, Z.; Liu, Y.; Wong, C. P. Facile fabrication of superhydrophobic octadecylamine-functionalized graphite oxide film. *Langmuir* **2010**, *26* (20), 16110−16114.
(49) Pham, V. H.; Dickerson, J. H. Superhydrophobic silanized melamine sponges as high efficiency oil absorbent materials. *ACS Appl. Mater. Interfaces* **2014**, *6* (16), 14181−14188.
(50) Merline, D. J.; Vukusic, S.; Abdala, A. A. Melamine formaldehyde: curing studies and reaction mechanism. *Polym. J.* **2013**, *45* (4), 413−419.
(51) Roach, P.; Shirtcliffe, N. J.; Newton, M. I. Progess in superhydrophobic surface development. *Soft Matter* **2008**, *4* (2), 224−240.
(52) Larmour, I. A.; Bell, S. E.; Saunders, G. C. Remarkably simple fabrication of superhydrophobic surfaces using electroless galvanic deposition. *Angew. Chem., Int. Ed.* **2007**, *46* (10), 1710−1712.
(53) Cassie, A. B. D.; Baxter, S. Wettability of porous surfaces. *Trans. Faraday Soc.* **1944**, *40*, 546−550.
(54) Wang, Z.; Elimelech, M.; Lin, S. Environmental applications of interfacial materials with special wettability. *Environ. Sci. Technol.* **2016**, *50* (5), 2132−2150.
(55) Singh, E.; Chen, Z.; Houshmand, F.; Ren, W.; Peles, Y.; Cheng, H. M.; Koratkar, N. Superhydrophobic graphene foams. *Small* **2013**, *9* (1), 75−80.
(56) Chu, Z.; Seeger, S. Superamphiphobic surfaces. *Chem. Soc. Rev.* **2014**, *43* (8), 2784−2798.
(57) Li, J. H.; Li, J. Y.; Meng, H.; Xie, S. Y.; Zhang, B. W.; Li, L. F.; Ma, H. J.; Zhang, J. Y.; Yu, M. Ultra-light, compressible and fire-resistant graphene aerogel as a highly efficient and recyclable absorbent for organic liquids. *J. Mater. Chem. A* **2014**, *2* (9), 2934−2941.
(58) Cheng, M.; Gao, Y.; Guo, X.; Shi, Z.; Chen, J.-f.; Shi, F. A Functionally integrated device for effective and facile oil spill cleanup. *Langmuir* **2011**, *27* (12), 7371−7375.
(59) Tran, D. N. H.; Kabiri, S.; Sim, T. R.; Losic, D. Selective adsorption of oil-water mixtures using polydimethylsiloxane (PDMS)-graphene sponges. *Environmental Science-Water Research & Technology* **2015**, *1* (3), 298−305.
(60) Wang, C.-F.; Lin, S.-J. Robust superhydrophobic/superoleophilic sponge for effective continuous absorption and expulsion of oil pollutants from water. *ACS Appl. Mater. Interfaces* **2013**, *5* (18), 8861−8864.
(61) Zhang, Z.; Sebe, G.; Rentsch, D.; Zimmermann, T.; Tingaut, P. Ultralightweight and flexible silylated nanocellulose sponges for the selective removal of oil from water. *Chem. Mater.* **2014**, *26* (8), 2659−2668.
(62) Mi, H. Y.; Jing, X.; Politowicz, A. L.; Chen, E.; Huang, H. X.; Turng, L. S. Highly compressible ultra-light anisotropic cellulose/graphene aerogel fabricated by bidirectional freeze drying for selective oil absorption. *Carbon* **2018**, *132*, 199−209.
(63) Wang, C. C.; Yang, S. D.; Ma, Q.; Jia, X.; Ma, P. C. Preparation of carbon nanotubes/graphene hybrid aerogel and its application for the adsorption of organic compounds. *Carbon* **2017**, *118*, 765−771.

DOI: 10.1021/acs.est.8b04642
Environ. Sci. Technol. 2019, 53, 1509−1517